Journal of Applied Electrochemistry **32**: 311–320, 2002.

Effect of complexing agents on the electrochemical behaviour of orthopaedic stainless steel in physiological solution

I. MILOŠEV
J. Stefan Institute, Department of Physical and Organic Chemistry, Jamova 39, 1001 Ljubljana, Slovenia

Received 5 July 2001; accepted in revised form 15 November 2002

Key words: complexing agents, cyclic voltammetry, physiological solution, stainless steel

Abstract

This work is aimed at providing a better understanding of the biocompatibility of stainless steel in the human body, where various biomolecules are able to bind metal ions and convey them from the surface of an orthopaedic implant to various parts of the body. The passivation behaviour of orthopaedic stainless steel was studied by potentiodynamic and potentiostatic electrochemical methods in physiological solution as a function of type and concentration of complexing agents added. The latter were used to simulate the complexing effect of biomolecules *in vitro*. Two complexing agents, EDTA and citrate, were investigated in the concentration range from 0.1 to 100 mM. Their addition induces a pronounced effect on the passivation characteristics of stainless steel. The results were discussed in the context of the formation of soluble complexes of metal ions, which induces an increase in metal dissolution and disturbs the formation of the passive layer. The degree of increased dissolution appears to be related to the stability constants of the complex formed.

1. Introduction

The passivation behaviour of stainless steels, the most important group of technological materials [1], has been investigated extensively [2–10]. It is now generally accepted that in neutral or slightly alkaline solutions a duplex passive film is formed, with an inner chromium oxide layer and an outer iron oxide layer [2–10]. The duplex nature of the passive film is reflected in its electronic structure, which can be represented by a heterojunction of p–n type [2]. The stoichiometry of the inner layer is approximately constant and corresponds to Cr_2O_3 [2–10]. The stoichiometry of iron oxide is a function of electrode potential and corresponds to different iron compounds: $Fe_3O_4(FeO \cdot Fe_2O_3)$ and $Fe(OH)_2$, at low potentials, and Fe_2O_3 and FeOOH at high potentials [2–10]. Nickel and molybdenum oxides also contribute to the passive film. The content of nickel in the form of NiO is generally found to be lower compared to that in the bulk alloy [5, 8, 10]. Some authors reported that Mo is enriched in the layer [8, 10], whereas others found the passive layer depleted in Mo [2, 11].

Among the numerous technological applications, stainless steels are used for medical applications. Type 316L stainless steel (ASTM F138 – 1986) contains 17–19% Cr, 13–15% Ni and 2–3 wt % Mo balanced with Fe and minor elements like Mn, C, P, S and Si [12]. This alloy is used for the manufacture of various orthopaedic devices, long-term implants such as hip and knee joint replacements, or short-term implants such as fixing plates for bone, screws and intramedullary rods. The biocompatibility of both permanent and temporary implants has always been a concern due the known adverse biological effects of individual metal components of stainless steel. Cr(VI) is toxic and carcinogenic, nickel is presumed to be carcinogenic and provokes contact dermatitis, whereas molybdenum induces anaemia [21]. *In vitro* studies on stainless steel have usually been performed in saline environment aimed at simulating physiological conditions [11, 13–15]. There have been few *in vitro* studies in serum solution [16–20]. The human body is a complex environment, containing not only passivating and aggressive species, but also species which act as complexing agents. For example, various proteins are able to bind metal ions and distribute them round the body [22]. The behaviour of stainless steel in the presence of complexing agents has not been investigated extensively.

There is thus a clear need for careful characterization of particular biocompatible metals under experimental conditions which closely simulate *in vivo* physiological conditions. In our previous paper the formation of the passive film on type 316L orthopaedic stainless steel in the presence of citrate as the complexing agent was studied by means of *in situ* X-ray photoelectron spectroscopy (XPS) [10]. Citrate affected the composition and thickness of the passive film. The present paper presents an electrochemical study of stainless steel and its metal components in simulated physiological solution (SPS) as a function of type and concentration of

complexing agents EDTA and citrate, which are used as model agents simulating the role of biomolecules *in vitro*.

2. Experimental details

Test specimens of orthopaedic stainless steel were cut from an original endoprosthesis (Protema-42, Protek, Sulzer, Switzerland). Their composition was confirmed by energy dispersive X-ray analysis (EDA) as follows: 61.4 at % Fe, 21.5 at % Cr, 14.7 at % Ni and 2.4 at % Mo. The following pure metals were used: Fe (99.5%), Cr (99.9%) by Johnson Matthey, and Ni (99%) and Mo (99.9%) by Goodfellow. Samples, 15 mm in diameter and 2 mm thick, were abraded down to 1000 SiC emery paper and rinsed with distilled water and acetone.

Prepared samples were embedded in a Teflon holder, so that an area of 0.785 cm^2 was exposed to the solution. Carbon rods and a saturated calomel electrode (SCE) served as counterelectrode and reference electrode, respectively. Potentials in the text refer to the SCE scale. Measurements were performed at 37 °C in simulated physiological solution (SPS): 8 g l^{-1} NaCl, 0.4 g l^{-1} KCl, 0.35 g l^{-1} $NaHCO_3$, 0.25 g l^{-1} $NaH_2PO_4 \times 2H_2O$, 0.06 g l^{-1} $Na_2HPO_4 \times 2H_2O$, 0.19 g l^{-1} $CaCl_2 \times 2H_2O$, 0.19 g l^{-1} $MgCl_2$, 0.06 g l^{-1} $MgSO_4 \times 7H_2O$, 1 g l^{-1} glucose, pH 7.8 (Hank's). The electrochemical cell had a capacity of 250 ml and was equipped with a water jacket.

The addition of EDTA (ethylendiaminetetraacetic acid disodium salt dihydrate) and citrate (tri-sodium citrate dihydrate) to SPS was studied at the following concentrations: 0.1, 1, 5, 10, 20, 50 and 100 mM. The addition of citrate did not change the pH value of the physiological solution. The addition of EDTA decreased the pH to 4.5, which was then adjusted back by the addition of NaOH.

Electrochemical measurements were carried out by means of a PAR&EGG (model 263) potentiostat/galvanostat controlled by M270 and M250 electrochemical software. Before starting the measurement, the samples were allowed to rest at the corrosion potential, E_{corr}, for one hour. Potentiodynamic polarization curves were started at −0.25 V with respect to the corrosion potential, E_{corr}, and progressed in the anodic direction with a potential scan rate of 1 mV s^{-1}. Cyclic voltammograms were recorded using potential scan rates between 5 and 100 mV s^{-1}. Potentiostatic transients were recorded for 200 s at each step of 0.1 V from −0.4 to 1.3 V. Integration of current density vs. time curves yielded the charge density.

3. Results

3.1. *Polarization curves for stainless steel and metal components*

Anodic polarization curves were recorded for stainless steel and its metal components in SPS with and without the addition of complexing agents EDTA and citrate over a concentration range from 0.1 to 100 mM. An example is given in Figure 1 for SPS with and without the addition of 50 mM EDTA. In SPS alone, iron is the most electronegative component with a corrosion potential, E_{corr}, of −0.7 V. It shows no tendency to passivation. Following the E_{corr}, the current density in the Tafel region increases exponentially with the potential and at −0.4 V reaches high values of limiting current density. The surface was covered by a black layer of Fe_3O_4 [23]. The E_{corr} of molybdenum at −0.35 V is followed by the Tafel region up to −0.2 V, where a narrow region of passivity at current density of 10^{-4} A cm^{-2} is established as a consequence of the formation of MoO_2 [23]. Nickel exhibits a somewhat broader passive range, from −0.35 V to −0.05 V, with lower current densities of 10^{-6} A cm^{-2} due to the formation of NiO [23]. The formation of a Cr_2O_3 layer on chromium is responsible for a broad passive range extending from −0.4 to 0.45 V, where it is interrupted by the process of transpassive oxidation [23]. Compared to its metal components, stainless steel exhibits the lowest values of current density and the broadest passivation range extending from −0.3 to 1.0 V.

The addition of EDTA induces significant changes in the polarization characteristics (Figure 1). A typical consequence is an increase in the current density and a shift of E_{corr} towards more negative values. The largest increase in current density is observed for iron, followed by that for nickel, molybdenum, chromium and stainless steel. Figure 2 shows the shift of the corrosion potential as a function of c_{EDTA} and $c_{citrate}$. In the case of iron, chromium, stainless steel and nickel, the corrosion potential shifts linearly towards more negative values, the slope decreasing in the same order, that is, from iron

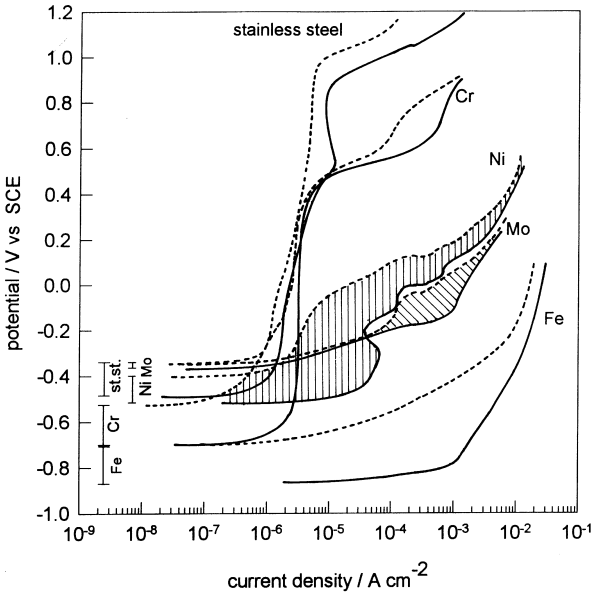

Fig. 1. Anodic polarisation curves recorded for stainless steel and its component metals in SPS with (——) and without (- - -) the addition of 50 mM EDTA. Scan rate 1 mV s^{-1}.

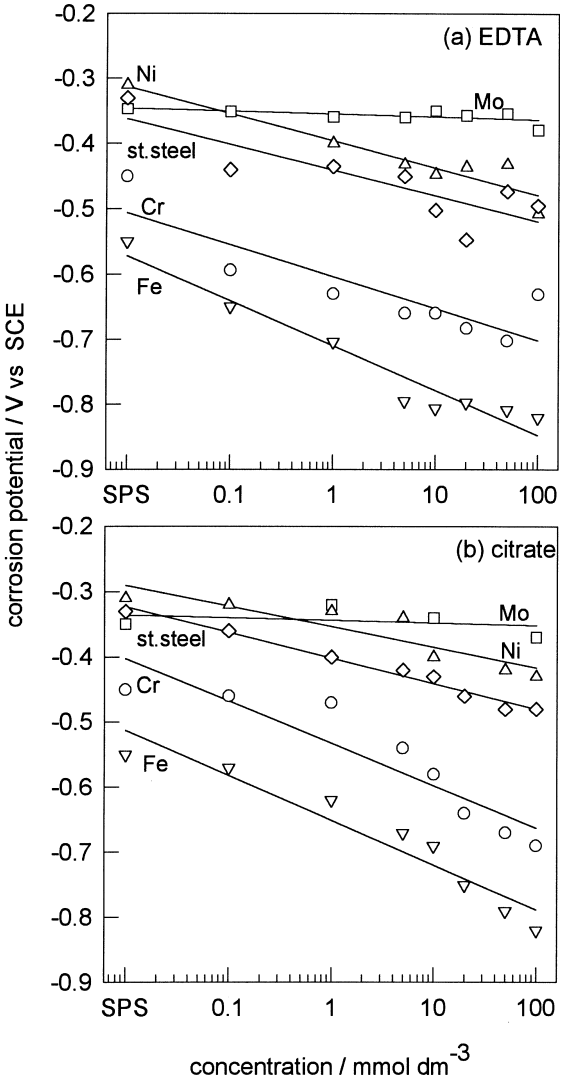

Fig. 2. Values of corrosion potential measured 1 h after immersion as a function of the concentration of (a) EDTA and (b) citrate added to SPS.

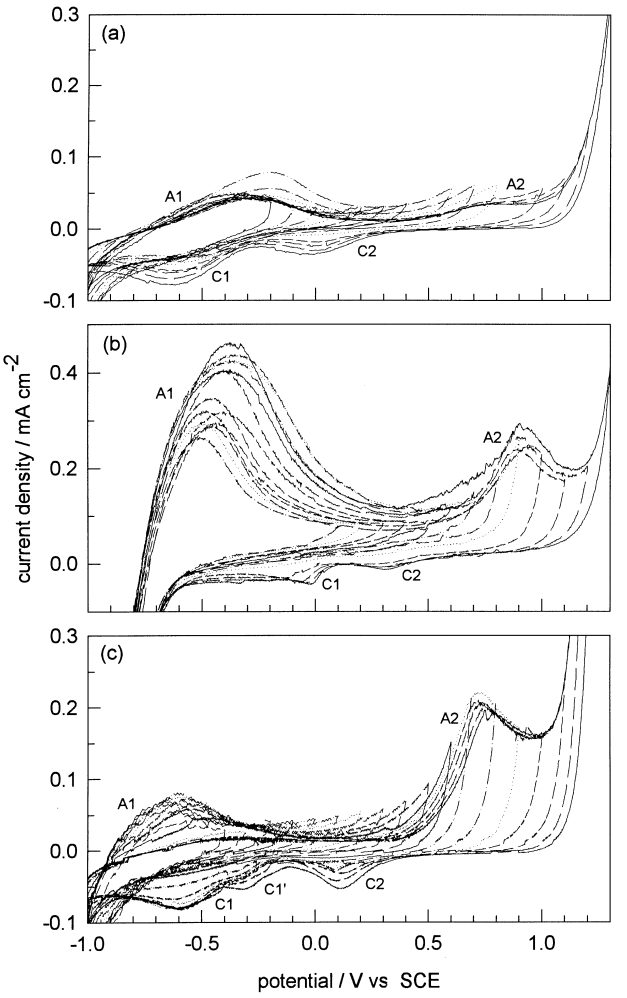

Fig. 3. Cyclic voltammograms recorded for stainless steel with increasing anodic potential scan limit, E_{an}, in (a) SPS alone and SPS containing (b) 50 mM EDTA and (c) 50 mM citrate. Scan rate 20 mV s^{-1}.

to nickel. In the case of molybdenum the values of E_{corr} are almost independent of c_{EDTA}.

3.2. *Influence of the anodic potential scan limit*

Cyclic voltammograms (CVs) recorded with increasing anodic potential scan limit, E_{an}, for stainless steel in SPS with and without 50 mM EDTA and 50 mM citrate are presented in Figure 3. The CV of stainless steel in SPS (Figure 3(a)) exhibits features which are in good agreement with those published under similar experimental conditions [11, 13–17]. The initial surface of stainless steel is not oxide-free due to the immediate formation of a thin layer of Cr_2O_3 in contact with air [10]. Three regions, passivating, passive and transpassive, are observed in the anodic cycle. Peak A1 at −0.3 V denotes the first region which can be ascribed mainly to the oxidation of iron to iron(II) oxide [10]. At higher potentials the stainless steel is passive, which may be ascribed to progressive formation of iron(III) oxide [10]. In the range from 0.7 to 1.1 V plateau A2 forms. At more positive potentials transpassive oxidation starts related mainly to the formation of Cr(VI) species [10]. In the cathodic cycle no peak is observed until E_{an} exceeds 0.5 V. For more positive E_{an}, the peak C1 starts to form at −0.6 V. This peak can be ascribed to the reduction of Fe(III) to Fe(II) species [24]. For $E_{an} > 0.9$ V, the peak C2 appears at 0 V, suggesting that peak C2 is related to the reduction of a product, primarily Cr(VI) species, generated during the transpassive oxidation at potentials exceeding that corresponding to peak A2. As E_{an} becomes more positive, the current density of cathodic peaks increases and their potentials shift slightly in the negative direction.

On addition of EDTA, the current density in the anodic cycle increases by the factor of ten (Figure 3(b)). The potential of peak A1 is shifted from −0.3 to −0.5 V. Its height increases markedly with increasing number of successive cycles. The plateau A2 is now transformed into a peak at 0.9 V. The appearance of peak C1 is delayed to $E_{an} > 0.9$ V, and that of peak C2 to $E_{an} > 1.0$ V.

Table 1. Ratio of total anodic charge to cathodic charge, Q_a/Q_c, deduced from cyclic voltammograms recorded for SPS with and without addition of 50 mM EDTA and citrate (Figure 3)

E_{an}/V	Charge ratio		
	SPS	SPS + citrate	SPS + EDTA
−0.3	0.3	1.1	3.6
−0.1	1.1	2.2	4.9
0.1	1.4	2.2	7.4
0.3	1.8	2.0	9.4
0.5	1.4	2.3	12.8
0.7	1.4	1.8	15.7
0.8	1.4	2.4	17.1
0.9	1.3	1.9	13.8
1.1	1.4	1.9	8.3
1.3	1.4	2.3	8.8

The potentials of the cathodic peaks are shifted in the positive direction; peak C1 now appears at 0 V, and peak C2 at 0.3 V. In contrast to the anodic peaks, the current density related to the cathodic peaks is approximately half the values measured in physiological solution.

In citrate containing solution the heights and potentials of the peaks A1, C1 and C2 are similar to those in SPS (Figure 3(c)). The current density of peak A1 increases with cycling, but not so intensively as in the case of EDTA. Peak A2 forms at 0.7 V. The potentials of cathodic peaks are somewhat more negative: peak C1 appears at −0.6 V for $E_{an} > 0.7$ V, and, for $E_{an} > 0.8$ V, a smaller hump C1′ appears at −0.3 V. For $E_{an} > 0.9$ V, peak C2 forms at 0.1 V.

Table 1 presents the dependence of the ratio of the total anodic and cathodic charges, Q_a/Q_c, as a function of anodic potential scan limit in SPS with and without addition of 50 mM EDTA and citrate. In SPS the value of Q_a/Q_c is close to 1, indicating almost quantitative reduction in the cathodic cycle. In SPS containing citrate the value of Q_a/Q_c increases to 2.4. The increase in charge ratio is more pronounced in the EDTA containing solution, where it increases dramatically and at 0.8 V reaches a value of 17.1 (compared to 1.4 and 2.4 in SPS and SPS containing citrate, respectively). This fact indicates that, in the presence of EDTA, a large amount of soluble species is formed in the anodic cycle. For $E_{an} > 0.8$ V the charge ratio decreases, which can be related to more pronounced cathodic reactions.

3.3. *Potentiostatic anodic transients*

Generally, in SPS the current density drops to low values at the beginning of the transient and then remains approximately constant, indicating passivation of the surface. For $E > 0.9$ V the current density starts to increase with time due to transpassive oxidation and oxygen evolution (Figure 3). With the addition of the complexing agent, and with the increase in its concentration, the current density, and consequently the deduced charge density, increases. For the same concentration of the two complexing agents, the increase in charge density is more pronounced for EDTA.

3.4. *Effect of the potential scan rate*

The effect of potential scan rate was investigated for all the concentrations of EDTA and citrate used. An example is given in Figure 4 for SPS and SPS containing 20 mM of EDTA and citrate. In SPS, current hysteresis is observed after potential reversal for the first two scan rates used, that is, 5 and 10 mV s^{-1} (Figure 4(a)). The current density continues to increase until it finally drops to zero at approximately −0.25 V. Consequently, the peak C2 is not observed in these two cycles. In subsequent scans the hysteresis disappears, indicating that a complete passivation of the surface is needed to prevent dissolution after the scan reversal. With increasing scan rate, the current density of the related peaks increases. The potential of peak A1 remains essentially unchanged, whereas the potentials of other peaks move only slightly, by 50 mV, towards more negative potentials. In the presence of EDTA, however, the potential

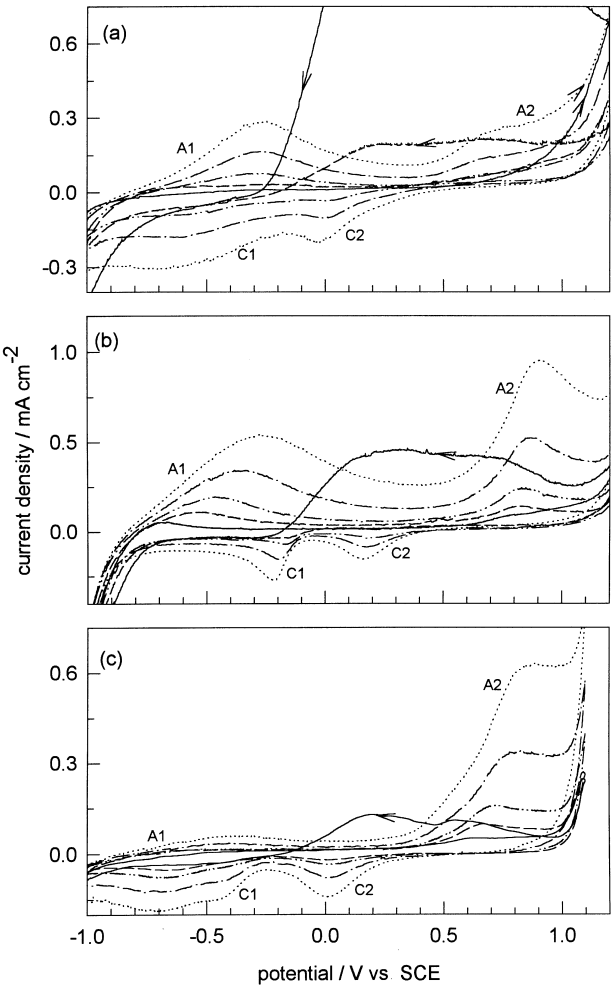

Fig. 4. Cyclic voltammograms recorded for stainless steel with increasing potential scan rate, dE/dt: 5, 10, 20, 50 and 100 mV s^{-1} in (a) SPS alone and SPS containing (b) 20 mM EDTA and (c) 20 mM citrate.

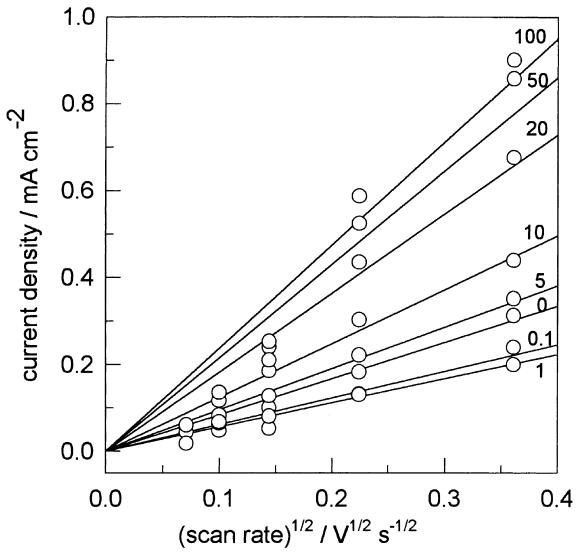

Fig. 5. The current density of the peak A1 as a function of the square root of the scan rate and c_{EDTA}.

of peak A1 is shifted to −0.7 V and with increasing scan rate moves significantly, by up to 500 mV, towards more positive values (Figure 4(b)). The shift of the potential of the peak A2 by up to 200 mV is not so pronounced. Cathodic peaks C1 and C2 move to about 100 mV more negative values with increasing scan rate. In contrast to the EDTA containing solution, the potential and current density of peak A1 are only slightly affected by the presence of citrate (Figure 4(c)). The shifts of other peaks are similar to those in EDTA containing solution.

The plot of the current density of peak A1 measured in EDTA containing solution against the square root of the scan rate, is linear and the slope increases with increasing concentration of EDTA (Figure 5). According to the Randles–Ševčik equation [25], the slope is given by $2.687 \times 10^5\, n^{3/2}\, c_0^{\infty} D^{1/2}$, where n is the number of electrons, and D is the diffusion coefficient ($cm^2\ s^{-1}$) and c_0^{∞} is the concentration of electroactive species in the bulk solution (mol cm^{-3}). Since it can be assumed that n and D are independent of the concentration of the complexing agent, the increase in slope is the consequence of an increase in the concentration of electroactive species in the solution.

3.5. *Effect of EDTA concentration on stainless steel and its metal components*

The addition of complexing agent was investigated in the concentration range from 0.1 to 100 mM. Figure 6 presents the CVs recorded for various concentrations of EDTA, with a scan rate of 20 mV s^{-1}. The heights of peaks A1 and A2 increase linearly with the logarithm of c_{EDTA}. In contrast to the anodic peaks, the heights of the cathodic peaks change only slightly with increasing c_{EDTA}. The shift of the peak potential as a function of

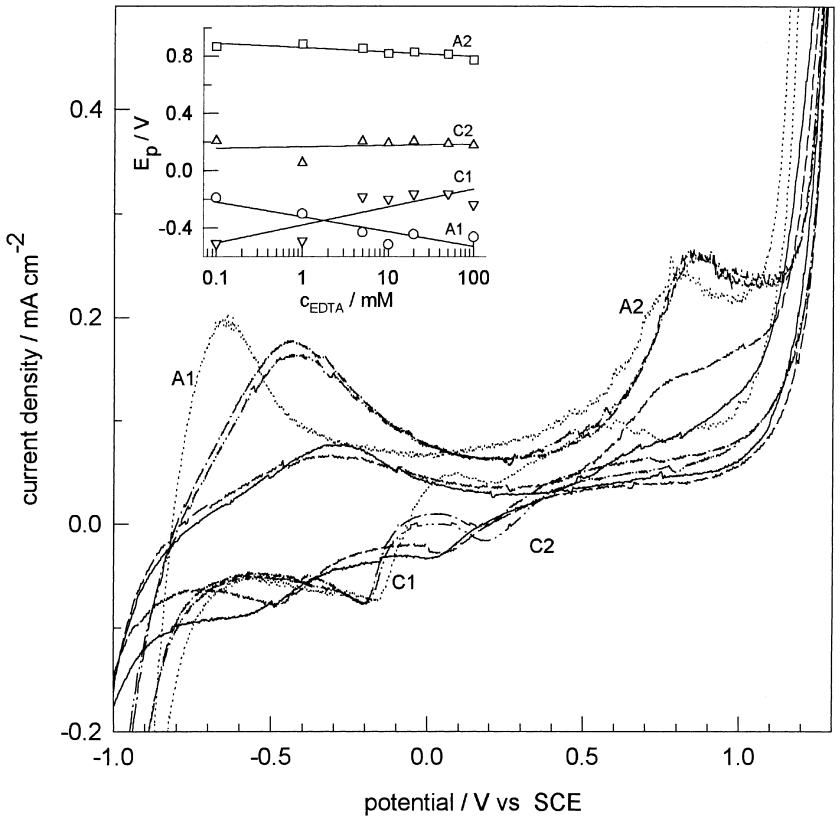

Fig. 6. Cyclic voltammograms recorded for stainless steel in SPS containing various concentrations of EDTA: 0 mM (——), 1 mM (- - - -), 5 mM (·····), 10 mM (-·-·-) and 50 mM (···). Scan rate 20 mV s^{-1}. Insert shows shift of the peak potential as a function of the log c_{EDTA}.

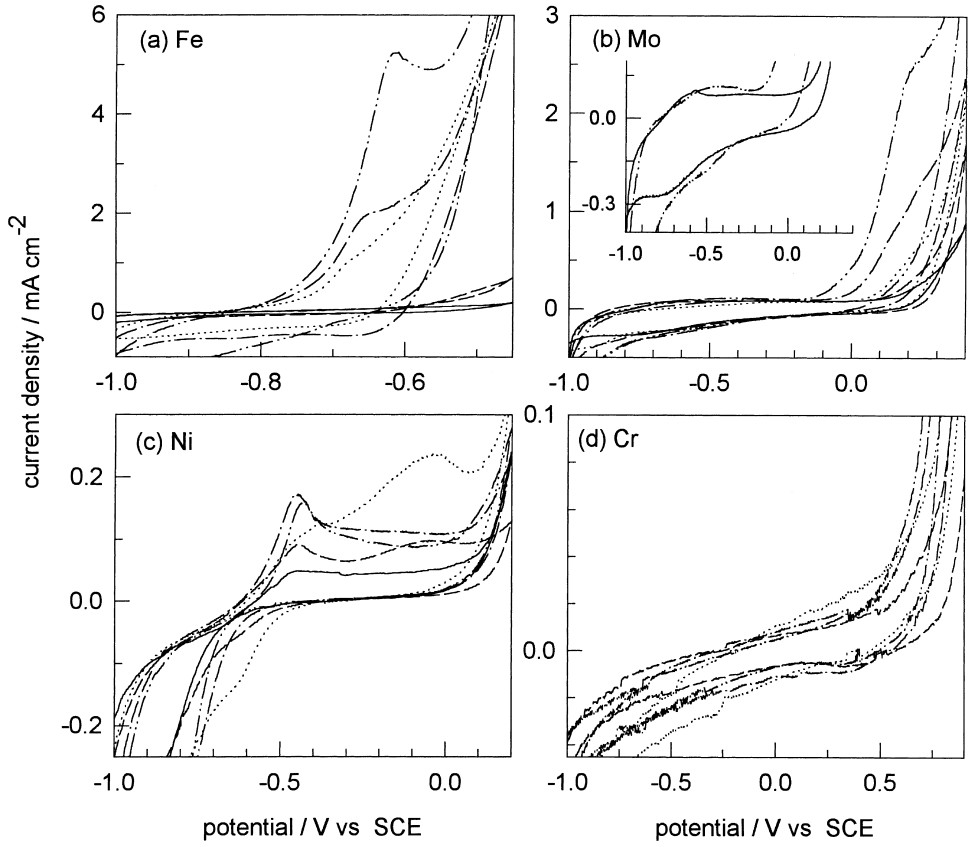

Fig. 7. Cyclic voltammograms recorded for pure metals: (a) iron, (b) molybdenum, (c) nickel and (d) chromium in SPS containing various EDTA concentrations: 0 mM (——), 1 mM (- - - -), 10 mM (·····), 20 mM (-·-·-) and 50 mM (-··-··-). Scan rate 20 mV s^{-1}.

the complexant concentration is shown in the insert. With increasing c_{EDTA} the potential of peak A1 shifts from −0.2 to −0.6 V. The potentials of peaks A2 and C2 are only slightly affected by c_{EDTA}. In SPS and SPS containing c_{EDTA} <5 mM peak C1 is located at −0.5 V and is rather broad. For $c_{EDTA} \geqslant 5$ mM, it becomes well defined and shifts to −0.2 V.

The origin of particular peaks in CVs of stainless steel may be partially identified from those recorded for constituent metals (Figure 7). The current density of iron in SPS is low up to −0.5 V, where it starts to increase steeply (Figure 7(a)). On the addition of EDTA the increase in current density occurs at more negative potentials and a peak forms progressively at −0.62 V. Its height increases with c_{EDTA} and is clearly related to the origin of peak A1 in the CV of stainless steel (Figure 6). In SPS molybdenum shows a very small peak at −0.6 V (insert in Figure 7(b)). The passive range is due to the formation of MoO_2 and/or MoO_3 and extends up to 0.1 V (Figure 7(b)) [23]. In the transpassive region, higher valency Mo(VI) species may be produced. On the addition of EDTA the anodic peak at −0.6 V becomes somewhat broader but does not change appreciably. Significant changes are observed at higher potentials, where the potential at which the transpassive region starts becomes progressively more negative (Figure 7(b)). The transpassive peak at 0.2 V is formed for $c_{EDTA} > 10$ mM. In physiological solution nickel exhibits a peak at −0.45 V followed by the low current density up to 0.15 V (Figure 7(c)). The passivation is based on the formation of a NiO layer [23]. The addition of EDTA increases the current density in the peak and in the passive range. At intermediate concentrations of EDTA (i.e., between 5 and 10 mM), a hump appears within the passive range around 0 V. The passivity of chromium is based on the formation of Cr_2O_3 [24]. Its stability is limited by the transpassive oxidation at 0.5 V (Figure 7(d)) and the accompanying formation of Cr(VI) species. For $E_{an} > 0.6$ V, a small cathodic peak appears at 0.4 V. This is related to reduction of the Cr(VI) species remaining incorporated in the layer [24]. The reduction peak at 0.4 V is clearly related to peak C2 of stainless steel (Figure 6), since it appears at similar potentials and is associated with the product generated during transpassive oxidation. The addition of EDTA does not appreciably affect the shape of the curve of chromium.

3.6. *Effect of citrate concentration on stainless steel and its metal components*

The effect of citrate on the passivation of stainless steel is less pronounced than that of EDTA (Figure 8). The height of peak A1 is similar to that in SPS and, in contrast to EDTA (Figure 6), is not affected significantly by $c_{citrate}$. The height of peak A2 is somewhat smaller than in EDTA containing solution and its potential is

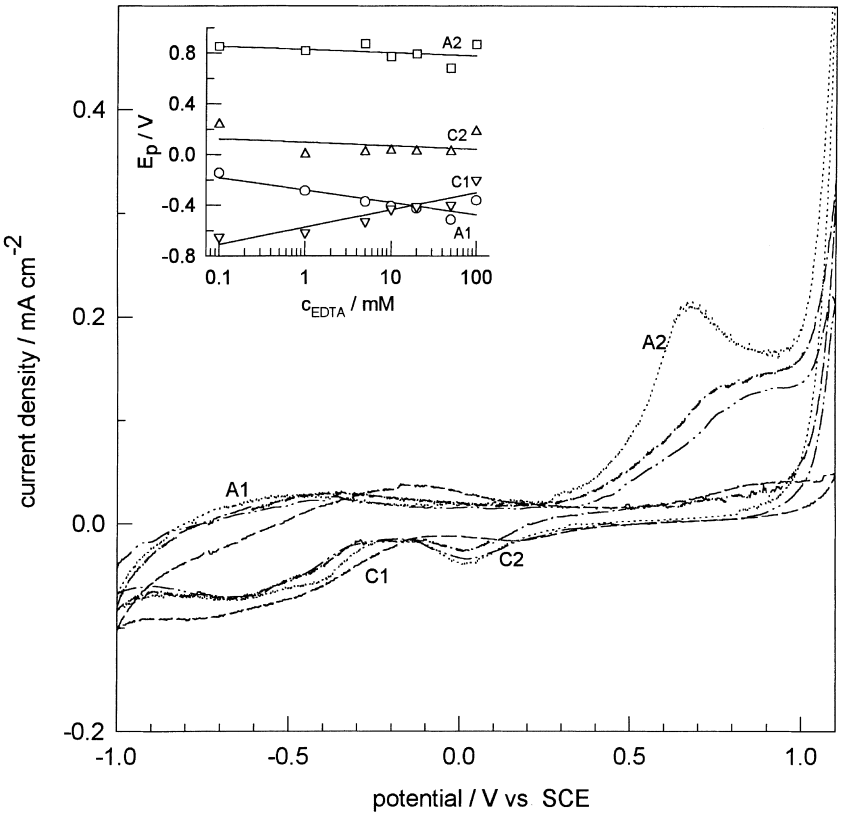

Fig. 8. Cyclic voltammograms recorded for stainless steel in SPS containing various concentrations of citrate: 0 mM (——), 1 mM (- - - -), 5 mM (·····), 10 mM (-·-·-) and 50 mM (·····). Scan rate 20 mV s^{-1}. Insert shows shift of the peak potential as a function of the log $c_{citrate}$.

slightly more negative. Its height increases linearly with $c_{citrate}$. The heights of cathodic peaks C1 and C2 are not significantly different from those in EDTA containing solution, but they form at somewhat more negative potentials. Their height is not appreciably affected by the citrate concentration. In contrast to EDTA, where peak C1 is shifted to −0.2 V for $c_{EDTA} > 5$ mM, in SPS containing citrate it remains unchanged for $c_{citrate} <$ 50 mM.

The cyclic voltammograms of individual pure metals in SPS containing various citrate concentrations are presented in Figure 9. The current density of iron increases with citrate concentration, but no anodic peak was observed as in the case of EDTA containing solution (Figure 9(a)). The addition of citrate shortens the passive region of molybdenum (Figure 9(b)) and no transpassive peak is observed. Nickel exhibits an anodic peak at −0.4 V, which changes only slightly with citrate concentration (Figure 9(c)). The behaviour of chromium is not significantly affected (Figure 9(d)).

4. Discussion

The contribution of individual metal components to the passivating film formed on stainless steel is not proportional to their content in the bulk alloy. Therefore, the behaviour of the alloy cannot be directly predicted from the behaviour of the individual metals. Iron oxides and chromium oxide are major constituents of the passive film and are responsible for the CV features of stainless steel. Nickel and molybdenum oxides are important, but minor, constituents of the film and their presence cannot be directly shown by CV of stainless steel. Comparison of the CVs of iron and stainless steel (Figures 6 and 7(a)) leads to the conclusion that peak A1 for stainless steel in SPS relates to iron oxidation. The rising slope of peak A1 is ascribed to the formation of Fe(II) species (Reaction 1, Table 2) [26–29], which may be further oxidized to Fe_3O_4 at slightly more positive potentials (Reaction 2). Iron in the alloy may also be oxidized directly (Reactions 3 and 4). In this lower potential region, where $E < 0$ V, Reactions 1 to 4 are the major ones occurring for iron in stainless steel in complexant-free SPS. The soluble corrosion product is in the form of Fe^{2+}, as proved by a rotating ring-disc study [24, 29]. By approaching the peak A2 the formation of higher-valency oxide Fe_2O_3 prevails [10, 26–31]. Since both have the structure of spinel, Fe_3O_4 can be easily transformed to γ-Fe_2O_3 (Reaction 5), or the latter can be formed directly from metal (Reaction 6). In this potential range, soluble corrosion products in the form of Fe^{3+} have been detected by a rotating ring-disc electrode [24, 29]. The contribution of nickel and molybdenum to the passive film on stainless steel should be taken into account [2, 4–10, 28]. Nickel in stainless steel enters the passive film as NiO at $E > 0.2$ V (Reaction 7) [10]. It is accumulated primarily at the

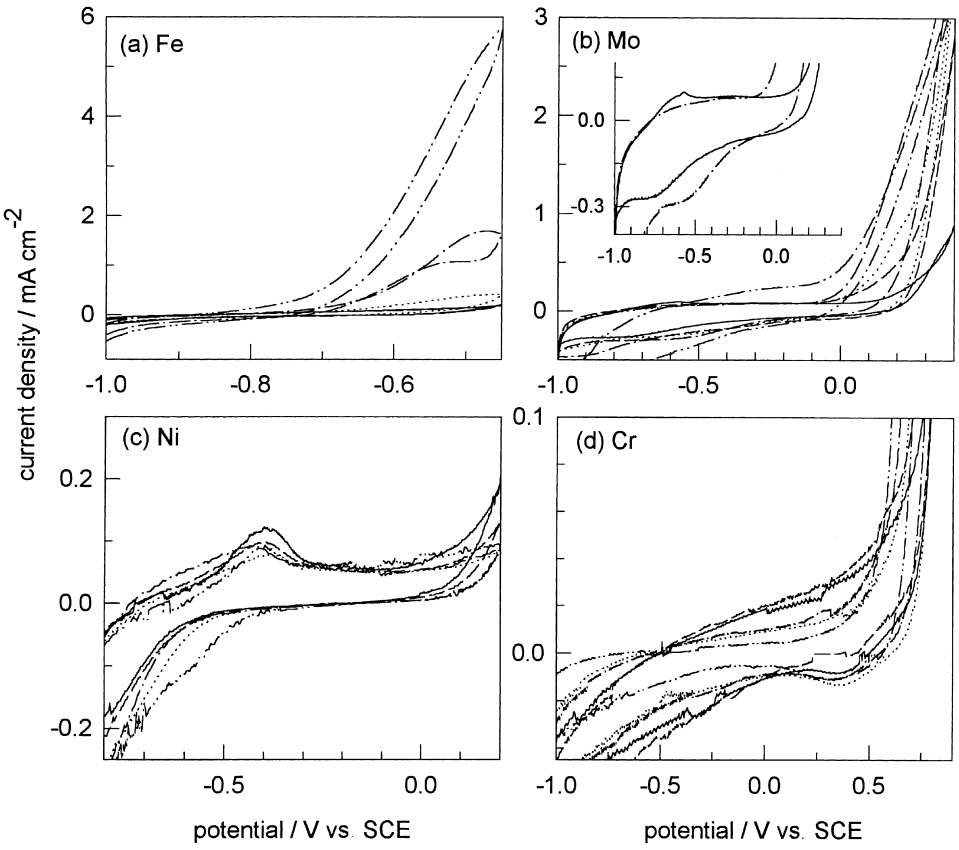

Fig. 9. Cyclic voltammograms recorded for pure metals: (a) iron, (b) molybdenum, (c) nickel and (d) chromium in SPS containing various citrate concentrations: 0 mM (——), 1 mM (- - - -), 10 mM (· · · ·), 20 mM (-·-·-) and 50 mM (-··-··-). Scan rate 20 mV s^{-1}.

Table 2. Possible reactions occurring at particular peaks in cyclic voltammograms of stainless steel [23]

Peak	No.	Reaction	Equilibrium potential
E < A1	1	$Fe \leftrightarrow Fe^{2+} + 2e^-$	$E_o = -0.440 + 0.0295 \log (Fe^{2+})$
	2	$3Fe^{2+} + 4H_2O \leftrightarrow Fe_3O_4 + 8H^+ + 2e^-$	$E_o = -0.980 - 0.236\ pH - 0.089 \log (Fe^{2+})$
	3	$Fe + H_2O \leftrightarrow FeO + 2H^+ + 2e^-$	$E_o = -0.047 - 0.059\ pH$
	4	$3Fe + 4H_2O \leftrightarrow Fe_3O_4 + 8H^+ + 8e^-$	$E_o = -0.085 - 0.059\ pH$
A1 < E < A2	5	$2Fe_3O_4 + H_2O \leftrightarrow 3Fe_2O_3 + 2H^+ + 2e^-$	$E_o = 0.221 - 0.059\ pH$
	6	$2Fe + 3H_2O \leftrightarrow Fe_2O_3 + 6H^+ + 6e^-$	$E_o = -0.051 - 0.059\ pH$
	7	$Ni + H_2O \leftrightarrow NiO + 2H^+ + 2e^-$	$E_o = 0.116 - 0.059\ pH$
	8	$Mo + 2H_2O \leftrightarrow MoO_2 + 4H^+ + 4e^-$	$E_o = -0.072 - 0.059\ pH$
E > A2	9	$Cr_2O_3 + 5H_2O \leftrightarrow 2CrO_4^{2-} + 10H^+ + 6e^-$	$E_o = 1.311 - 0.098\ pH + 0.019 \log (CrO_4^{2-})$
	10	$Ni(II) + 2H_2O \leftrightarrow NiO_2 + 4H^+ + 2e^-$	$E_o = 1.593 - 0.118\ pH - 0.029 \log (Ni^{2+})$
	11	$MoO_2 + 2H_2O \leftrightarrow MoO_4^{2-} + 4H^+ + 2e^-$	$E_o = 0.606 - 0.118\ pH + 0.029 \log (MoO_4^{2-})$
C2	12	$Cr_2O_3 + 5H_2O \leftrightarrow 2CrO_4^{2-} + 10H^+ + 6e^-$	$E_o = 1.311 - 0.098\ pH + 0.019 \log (CrO_4^{2-})$
C1	13	$2Fe(II) + 3H_2O \leftrightarrow Fe_2O_3 + 6H^+ + 2e^-$	$E_o = 0.728 - 0.177\ pH - 0.059 \log (Fe^{2+})$

metal surface and its content in the oxide layer is less than that in the bulk. As for nickel, no particular feature in the CV of stainless steel can be ascribed directly to the oxidation of Mo. Analysis of the surface [10] has proved that Mo enters the passive film at $E > 0$ V (Reaction 8). It is enriched compared to its content in the bulk. The reactions occurring at potentials exceeding peak A2 ($E > 0.8$ V) are related to transpassive processes. The inner layer of Cr_2O_3 undergoes oxidation, resulting in the formation of Cr(VI) species (Reaction 9). Furthermore, transpassive oxidation of Ni and Mo may also occur (Reactions 10 and 11) [28]. In the reverse cycle, Cr(VI) species which remain incorporated in the oxide layer are reduced to Cr(III) in the region of peak C2 (Reaction 12) [2–10, 27, 28]. The reduction peak C1 corresponds to the reduction of Fe_2O_3 to Fe(II) species, which then dissolves into solution (Reaction 13) [3, 24, 26–29].

In the presence of the complexing agent, complexation reactions also have to be taken into consideration. It is known that EDTA (H_4Y) forms complexes with both Fe(II) and Fe(III) species (Table 3) [32]. A soluble corrosion product in the form of Fe^{2+} released in the lower potential range [24, 29] may be complexed by

Table 3. Logarithm of stability constants, log K_{st}, of complexes of EDTA and citrate with metal cations for the reaction $M + L \leftrightarrow ML$, where M is the metal cation and L is the ligand [32]

Ligand	log K_{st}		
	Fe^{2+}	Fe^{3+}	Ni^{2+}
EDTA	14.3	25.1	18.5
Citrate	4.4	11.5	5.3

EDTA. The formation of relatively strong complexes, possibly of the type FeY^{2-}, with a logarithm of stability constant, log K_{st}, of 14.32 may be expected (Table 3). Due to the rapid formation of complexes with high stability constant, the equilibrium of Reaction 1 from Table 2 is shifted to the right, thus promoting the dissolution of iron. The formation of a large amount of dissolved iron species in this potential range is supported by the increase in the current density of peak A1 with increasing c_{EDTA} (Figures 3 and 6) and by a marked increase in the ratio of total anodic to cathodic charges, Q_a/Q_c (Table 1). Figure 5 demonstrates the increase in the concentration of electroactive species in the solution due to increasing c_{EDTA}. Moreover, the increased concentration of soluble corrosion product in the presence of EDTA has been demonstrated by differential pulse polarography [20]. As the consequence of the increased dissolution into solution, the formation of solid oxide layer is delayed and its composition is changed. *In situ* XPS measurements have confirmed that, in the lower potential range (i.e., $E < 0$ V), the oxide layer is thinner and markedly depleted in iron [10].

With increasing concentration of EDTA, the current density in the potential range approaching the peak A2 increases strongly (Figure 6) due to the formation of very strong complexes with Fe^{3+} (Table 3). Fe^{3+} is the dissolution product formed in this potential range from the main oxide layer Fe_2O_3 [24, 29]. EDTA also forms strong complexes with Ni^{2+}, which may additionally contribute to the increase in current density. Ni^{2+} is the dissolution product formed in this potential range from minor oxide constituent NiO [28].

The addition of EDTA does not appreciably affect the shape of the curve of chromium. EDTA forms strong complexes with Cr^{3+} ions in free solution with the log K_{st} of 23.4 [32]. However, the amount of dissolved Cr(III) species available for complexation is extremely small [20] presumably due to very slow dissolution of a strongly protective Cr_2O_3 layer. Furthermore, Cr(III) ions are known for their extremely slow rate of exchange with ligands in the first coordination shell [33, 34]. The small effect of EDTA on the behaviour of chromium is in accordance with experimentally observed independence of the height and the potential of peak C2 of the c_{EDTA}.

Besides an increase in current density, the second typical characteristic related to the addition of complexing agent is the shift of the peak potential. The addition of EDTA induces a strong shift of the anodic peak A1 towards more negative values (Figures 3 and 6). This fact can be explained by the dependence of the equilibrium potential, E_o, of Reaction 1 (Table 2) on the concentration of Fe^{2+} species. The latter will be dependent on the concentration of the complexing agent and on the stability constant of the complex. Therefore, the concentration of ligand would be expected to affect the value of equilibrium potential by changing the concentration of dissolved species.

Sakakibara et al. have studied iron in anhydrous methanol solution containing various basic and acidic complexing agents [35]. The stimulation of the anodic process was closely related to the stability constant of the complex. The results presented here agree well with literature data [35, 36]. Both EDTA and citrate affect the passivation behaviour of stainless steel, but to different extents. This may be explained by the different stability constants of complexes of the metal ions with EDTA and citrate [32]. Citrate is a far less strong complexant for Fe(II) (Table 3). This may be reflected in the smaller current density of peak A1, which denotes the dissolution and formation of Fe(II) species (Figures 6 and 8). The shift in the corrosion potential is smaller than in the case of EDTA (Figure 2). On the other hand, peak A2 increases in the presence of citrate, as observed for EDTA. Compared to Fe(II), Fe(III) forms stronger complexes with citrate (Table 3) and since in this potential range the soluble species are in the form of Fe(III), it may be assumed that their complexation with citrate becomes significant.

5. Conclusions

The behaviour of stainless steel and individual metal components was studied in simulated physiological solution by potentiodynamic and potentiostatic electrochemical methods with and without the addition of complexing agents EDTA and citrate. Generally, the passivation of stainless steel in physiological solution is based on the formation of a layer containing two major oxides: chromium and iron oxide. The oxides of nickel and molybdenum may also be included in the passive film as minor constituents. The complexing agents have a profound effect on the behaviour of stainless steel. The anodic process is stimulated by dissolution at the surface caused by the formation of soluble complexes. This process is demonstrated by the increased current density of the anodic peaks, and the shift of the peak potential. The formation of a large amount of soluble metal species in solution is supported by the strong increase in ratio of anodic to cathodic charges.

The degree of stimulation of anodic dissolution is a function of the type of complexing agent, and its concentration. Fe(II), Fe(III) and Ni(II) form relatively strong complexes with EDTA, whereas citrate forms the strongest complexes with Fe(III). The observed electrochemical results demonstrate that the stability constants

of the particular complexes formed affect the degree of stimulation of the anodic dissolution.

The knowledge of the effect of complexing agents on the corrosion resistance would provide a better understanding of processes occurring *in vivo* on the surface of stainless steel. This paper presents a model study for the investigation of the stainless steel in the presence of biomolecules which *in vivo* act as complexing agents.

Acknowledgements

The author would like to thank Ms. Anita Zajc for her skilful and careful technical work. This work forms part of the project financed by the Ministry of Science and Technology Republic of Slovenia (Projects PS-544 and J3-7838).

References

1. R. Green (Ed.), 'The Chemical Engineering Guide to Corrosion' (McGraw-Hill, New York, 1986), pp. 162–192.
2. N.E. Hakiki, M. Da Cunha Belo, A.M.P. Simões and M.G.S. Ferreira, *J. Electrochem. Soc.* **145** (1998) 3821.
3. C. Calinski and H-H. Strehblow, *J. Electrochem. Soc.* **136** (1989) 1328.
4. R.F.A. Jargelius-Pettersson and B.G. Pound, *J. Electrochem. Soc.* **145** (1998) 1462.
5. G. Lorang, M. Da Cunha Belo, A.M.P. Simões and M.G.S. Ferreira, *J. Electrochem. Soc.* **141** (1994) 3347.
6. N. Ramasubramanian, N. Preocanin and R.D. Davidson, *J. Electrochem. Soc.* **132** (1985) 793.
7. I. Olefjord, B. Brox and U. Jelvestam, *J. Electrochem. Soc.* **132** (1985) 2854.
8. A. Rossi and B. Elsener, Proceedings of the 12th International Corrosion Congress (1993), pp. 2120–2130.
9. Z. Szklarska-Smialowska, 'Pitting Corrosion of Metals' (NACE, Houston, TX, 1986), pp. 143–157.
10. I. Milošev and H-H. Strehblow, *J. Biomed. Mater. Res.* **52** (2000) 404.
11. Y. Okazaki, T. Tateishi and I. Yoshimasa, *Mater. Trans. JIM* **38** (1997) 78.
12. 'Annual Book of ASTM Standards', vol. 13.01. 'Medical Devices' (ASTM, Philadelphia, 1988), pp. 26–28.
13. P. Kovacs, Proceeding of the NACE Annual Conference and Corrosion Show (1992), paper 214.
14. M. Sivakumar, U. Kamachi and S. Rajeswari, *J. Mater. Eng. Perf.* **3** (1994) 744.
15. J. Pan, C. Karlen and C. Ulfvin, *J. Electrochem. Soc.* **147** (2000) 1021.
16. K. Meinert and G.K. Wolf, *Surf. Coat. Technol.* **98** (1998) 1148.
17. T. Moura e Silva, J.M. Monteiro, M.G.S. Ferreira and J.M. Vieira, *Clin. Mater.* **12** (1993) 103.
18. K. Merritt and S. Brown, *J. Biomed. Mater. Res.* **22** (1988) 111.
19. K. Merritt, S.A. Brown and N.A. Sharkey, *J. Biomed. Mater. Res.* **18** (1984) 1005.
20. A. Minovič, I. Milošev and B. Pihlar, submitted to *J. Mater. Sci: Materials in Medicine*.
21. B.F. Morrey (Ed.), 'Biological, Material, and Mechanical Considerations of Joint Replacement' (Raven Press, New York, 1993).
22. J. Yang and J. Black, *Biomaterials* **15** (1994) 262.
23. M. Pourbaix 'Atlas of Electrochemical Equilibria in Aqueous Solutions' (NACE, Cebelcor, Houston, Brussels, 1974).
24. S. Haupt and H-H. Strehblow, *Langmuir* **3** (1987) 873.
25. P. Delahay, 'New Instrumental Methods in Electrochemistry' (Interscience, New York, London, 1954), pp. 115–145.
26. M. Nagayama and M. Cohen, *J. Electrochem. Soc.* **109** (1962) 781.
27. C.A. Melendres and M. Pankuch, Y.S. Li, R.L. Knight, *Electrochim. Acta* **37** (1992) 2747.
28. T. Piao T and S-M. Park, *J. Electrochem. Soc.* **144** (1997) 3371.
29. H. Zhang and S-M. Park, *J. Electrochem. Soc.* **141** (1994) 718.
30. M. Cohen, D. Mitchell and K. Hashimoto, *J. Electrochem. Soc.* **126** (1979) 442.
31. W-C. Baek, T. Kang, H-J. Sohn and Y.T. Kho, *Electrochim. Acta* **46** (2001) 2321.
32. R.M. Smith and A.E. Martell (Eds), 'Critical Stability Constants', vol. 3 (Plenum Press, New York London, 1977), p. 163.
33. H-H. Strehblow, *in* P. Marcus and J. Oudar (Eds), 'Corrosion Mechanisms in Theory and Practice' (Marcel Dekker, New York, 1995), pp. 201–237.
34. F.A. Cotton and G. Wilkinson (Eds), 'Advanced Anorganic Chemistry', 5th edn (Wiley-Interscience, New York, 1988), p. 40.
35. M. Sakakibara, H. Nishihara and K. Aramaki, *Corrosion Sci.* **34** (1993) 1937.
36. M.A. Khan, R.L. Williams and D.F. Williams, *Biomaterials* **20** (1999) 631.